Hygrothermal analysis of multilayered composite plates by variable kinematic finite elements

Hygro-thermal analysis of multilayered composite plates by variable kinematic finite elements

M. Cinefra, M. Petrolo, G. Li and E. Carrera

MUL^2 Group, Department of Mechanical and Aerospace Engineering,
Politecnico di Torino, Corso Duca degli Abruzzi 24, 10129 Torino, Italy.

Submitted to Journal of Thermal Stresses

Keywords:
finite elements, Carrera Unified Formulation, hygrothermal, trigonometric, exponential, plate.

Author and address for Correspondence
Dr. Maria Cinefra
Associate Professor,
MUL^2 Group, Department of Mechanical and Aerospace Engineering
Politecnico di Torino,
Corso Duca degli Abruzzi, 24,
10129 Torino, ITALY,
tel +39 011 090 6845, fax +39 011 090 6899
e.mail: maria.cinefra@polito.it

Abstract

Advanced plate models with variable kinematics for steady state hygrothermal analysis of composite laminates are proposed. The refined models discussed include both Layer-Wise (LW) and Equivalent Single Layer (ESL) models, and the Carrera Unified Formulation (CUF) is used. The Mixed Interpolation of Tensorial Component (MITC) method is applied to a nine-node element to contrast the shear locking phenomena. The governing equations are derived from the Principle of Virtual Displacement (PVD) taking into account elastic mechanical, thermal and hygroscopic effects. Through-the-thickness variations of temperature and moisture concentration are calculated by solving the Fourier equation and the Fick law, respectively. Cross-ply plates with symmetrical lamination and simply supported edges subjected to bisinusoidal thermal/hygroscopic loads are analyzed considering various thickness ratios. Results obtained with assumed linear and calculated temperature/hygroscopic profiles are compared. Variable kinematics with a variety of thickness functions are compared regarding both accuracy and computational costs. The results show that all the kinematics proposed can approximate the transverse shear stress distribution through the thickness with satisfactory accuracy when sufficient expansion terms are adopted. In some cases, miscellaneous expansions can lead to significant reductions in computational costs. The results here presented can be used as benchmark solutions for future works.

Introduction

Laminated structures like composite plates have been widely used in aerospace engineering. Such structures often undergo environmental conditions, e.g. high temperature, and humidity. Hygrothermal effects can lead to the reduction in both constitutive properties and strength of fiber reinforced polymer composites [1, 2]. The possible high hygrothermal residual stress state is also a serious issue in the design of laminated composite structures. Efficient mechanical models with the ability to capture the hygrothermal elastic behaviors of multilayered structures are of great significance. Closed form analytical solutions are only available in several cases, making numerical methods such as FEM the first choice for engineering applications.

Studies on thermal elastic behaviors of composite laminates have been reported by many authors. With the linear temperature profile assumption, Kant [3] and Khdeir [4] considered this problem with first-order theories. The significance of mixed models for accurate estimations of transverse shear/normal stresses under thermal load has been remarked in [5] and [6].

The thermal conduction in solid media can be described by the Fourier equation, which can be solved by adopting the methodology proposed by Tungikar [7]. Concerning thermal elastic analysis of composite laminates, Carrera [8] exploited the partially coupled thermal elastic governing equations and discussed the influence of through-the-thickness variation of temperature by comparing the thermal mechanical response of laminated anisotropic plates; in particular, assumed profiles and calculated profiles obtained by solving the Fourier conduction equation were used. For thin laminated structures, calculated steady state through-the-thickness temperature profiles can be very close to an assumed linear one, while this is not the case for thick laminates [8]. Fully coupled thermo mechanical analyses on laminated plates can be found in [9].

Following Fourier's work [10], Fick pointed out that the diffusion of moisture in solid media follows the same rule as heat does [11]. Moreover, researchers pointed out that thermal conduction coefficients and humidity diffusivity depend on the temperature [2]. Generally speaking, there is an interaction between thermal environment and moisture diffusion[2], but the temperature approaches equilibrium much faster than moisture concentration [12, 13]. By considering the analogy between thermal conduction and moisture diffusion, Szekeres et al. [14, 15] suggested that the methodology used to solve the Fourier equation [7] can be extended to hygroscopic problems, which has been the basis of many later works.

Benkeddad [16, 17] studied the moisture diffusion process in composite plates by taking only the thickness dimension into consideration, leading to a 1D diffusion problem, and the moisture concentration at a given moment was determined by finite difference method. A similar methodology was adopted for the analysis of transient hygroscopic stresses in unidirectional laminated composite plates with cyclic and asymmetrical environmental conditions by Tounsi et al. [18–21]. Abbas [22] and Boukhoulda [23] introduced the Laplace transform to obtain analytical solutions for transient moisture concentration problems. Patel [24] and Lo et al. [25] considered the variation of material properties due to temperature and moisture variation for the static response analysis of multilayered plates.

Carrera Unified Formulation (CUF) provides a methodology to develop refined models for the analysis of laminated composite structures, enabling FEM models to have variable kinematics of arbitrary order. Many advanced FEM models have been proposed and applied but not restricted to multifield problems. Carrera [26, 27] proposed advanced finite elements for composite laminates based on CUF using both Equivalent Single Layer (ESL) and Layer-Wise (LW) approaches. Trigonometric trial functions were used in combination with Ritz method in [28].

In authors' previous works [29], CUF was applied to thermoelastic problems of laminated structures, and their static bending responses under both assumed linear and calculated temperature profiles, obtained by solving the Fourier equation, were reported. The Mixed Interpolation of Tensorial Components (MITC) [30–33] method was implemented to alleviate lockings. Such an MITC9 element with a variety of thickness functions have been used to investigate the static response of cross-ply laminated plates and shells [34].

In this paper, considering the analogy between moisture diffusion and thermal conduction, the approach that has been successfully used in solving heat conduction problems [29] is extended to steady state hygroelastic problems. This study mainly focuses on the performance of variable and miscellaneous kinematics of plate elements in the analysis of hygrothermal problems. For simplicity, it is assumed that the thermal conductivity and mass diffusivity do not change with temperature. Both the thermal and hygroscopic problems are restricted to steady state conditions.

Geometrical and constitutive relations

The reference system and the geometry of the multilayered plate are given in Fig. 1.

Considering a multilayered structure, where the index k indicates the layer, the geometrical relations can be written as:

$$\begin{aligned} \boldsymbol{\epsilon}_p^k &= \left\{ \epsilon_{xx}^k, \epsilon_{yy}^k, \epsilon_{xy}^k \right\}^T = \boldsymbol{D}_p \boldsymbol{u}^k \\ \boldsymbol{\epsilon}_n^k &= \left\{ \epsilon_{xz}^k, \epsilon_{yz}^k, \epsilon_{zz}^k \right\}^T = (\boldsymbol{D}_{n\Omega} + \boldsymbol{D}_{nz}) \boldsymbol{u}^k \end{aligned} \tag{1}$$

The explicit form of the introduced arrays, that contain differential operators, is:

$$\boldsymbol{D}_p = \begin{bmatrix} \partial_x & 0 & 0 \\ 0 & \partial_y & 0 \\ \partial_y & \partial_x & 0 \end{bmatrix}, \quad \boldsymbol{D}_{n\Omega} = \begin{bmatrix} 0 & 0 & \partial_x \\ 0 & 0 & \partial_y \\ 0 & 0 & 0 \end{bmatrix}, \quad \boldsymbol{D}_{nz} = \begin{bmatrix} \partial_z & 0 & 0 \\ 0 & \partial_z & 0 \\ 0 & 0 & \partial_z \end{bmatrix}. \tag{2}$$

Considering the expansion caused by the increase of temperature and moisture absorption, the strain vector can be expressed as follows:

$$\begin{aligned} \boldsymbol{\epsilon}_p^k &= \boldsymbol{\epsilon}_{pu}^k - \boldsymbol{\epsilon}_{p\theta}^k - \boldsymbol{\epsilon}_{p\eta}^k \quad &= \boldsymbol{\epsilon}_{pu}^k - \boldsymbol{\alpha}_p^k \theta^k - \boldsymbol{\beta}_p^k \eta^k \\ \boldsymbol{\epsilon}_n^k &= \boldsymbol{\epsilon}_{nu}^k - \boldsymbol{\epsilon}_{n\theta}^k - \boldsymbol{\epsilon}_{n\eta}^k &= \boldsymbol{\epsilon}_{nu}^k - \boldsymbol{\alpha}_n^k \theta^k - \boldsymbol{\beta}_n^k \eta^k \end{aligned} \tag{3}$$

where α_{ij} are the thermal expansion coefficients, and β_{ij}^k the moisture expansion coefficients, which in an explicit form are:

$$\begin{aligned} \boldsymbol{\alpha}_p^k &= \begin{Bmatrix} \alpha_1^k & \alpha_2^k & 0 \end{Bmatrix}^T, \quad \boldsymbol{\alpha}_n^k = \begin{Bmatrix} 0 & 0 & \alpha_3^k \end{Bmatrix}^T \\ \boldsymbol{\beta}_p^k &= \begin{Bmatrix} \beta_1^k & \beta_2^k & 0 \end{Bmatrix}^T, \quad \boldsymbol{\beta}_n^k = \begin{Bmatrix} 0 & 0 & \beta_3^k \end{Bmatrix}^T \end{aligned} \tag{4}$$

θ indicates the increment of temperature, and η the moisture absorption. The stress-strain relations are:

$$\begin{aligned} \boldsymbol{\sigma}_p^k &= \begin{Bmatrix} \sigma_{xx}^k, \sigma_{yy}^k, \sigma_{xy}^k \end{Bmatrix}^T = \boldsymbol{\sigma}_{pu}^k - \boldsymbol{\sigma}_{p\theta}^k - \boldsymbol{\sigma}_{p\eta}^k = \boldsymbol{C}_{pp}^k \boldsymbol{\epsilon}_{pu}^k + \boldsymbol{C}_{pn}^k \boldsymbol{\epsilon}_{nu}^k - \boldsymbol{\lambda}_p^k \theta^k - \boldsymbol{\mu}_p^k \eta^k \\ \boldsymbol{\sigma}_n^k &= \begin{Bmatrix} \sigma_{xz}^k, \sigma_{yz}^k, \sigma_{zz}^k \end{Bmatrix}^T = \boldsymbol{\sigma}_{nu}^k - \boldsymbol{\sigma}_{n\theta}^k - \boldsymbol{\sigma}_{n\eta}^k = \boldsymbol{C}_{np}^k \boldsymbol{\epsilon}_{pu}^k + \boldsymbol{C}_{nn}^k \boldsymbol{\epsilon}_{nu}^k - \boldsymbol{\lambda}_n^k \theta^k - \boldsymbol{\mu}_n^k \eta^k \end{aligned} \tag{5}$$

where

$$\begin{aligned} \boldsymbol{C}_{pp}^k &= \begin{bmatrix} C_{11}^k & C_{12}^k & C_{16}^k \\ C_{12}^k & C_{22}^k & C_{26}^k \\ C_{16}^k & C_{26}^k & C_{66}^k \end{bmatrix} \qquad \boldsymbol{C}_{pn}^k = \begin{bmatrix} 0 & 0 & C_{13}^k \\ 0 & 0 & C_{23}^k \\ 0 & 0 & C_{36}^k \end{bmatrix} \\ \boldsymbol{C}_{np}^k &= \begin{bmatrix} 0 & 0 & 0 \\ 0 & 0 & 0 \\ C_{13}^k & C_{23}^k & C_{36}^k \end{bmatrix} \qquad \boldsymbol{C}_{nn}^k = \begin{bmatrix} C_{55}^k & C_{45}^k & 0 \\ C_{45}^k & C_{44}^k & 0 \\ 0 & 0 & C_{33}^k \end{bmatrix} \end{aligned} \tag{6}$$

$$\begin{cases} \boldsymbol{\lambda}_p^k = \boldsymbol{C}_{pp}^k \boldsymbol{\alpha}_p^k + \boldsymbol{C}_{pn}^k \boldsymbol{\alpha}_n^k \\ \boldsymbol{\lambda}_n^k = \boldsymbol{C}_{np}^k \boldsymbol{\alpha}_p^k + \boldsymbol{C}_{nn}^k \boldsymbol{\alpha}_n^k \end{cases} \tag{7}$$

$$\begin{cases} \boldsymbol{\mu}_p^k = \boldsymbol{C}_{pp}^k \boldsymbol{\beta}_p^k + \boldsymbol{C}_{pn}^k \boldsymbol{\beta}_n^k \\ \boldsymbol{\mu}_n^k = \boldsymbol{C}_{np}^k \boldsymbol{\beta}_p^k + \boldsymbol{C}_{nn}^k \boldsymbol{\beta}_n^k \end{cases} \tag{8}$$

where $\boldsymbol{\lambda}_p^k$ and $\boldsymbol{\lambda}_n^k$ are the vectors of thermomechanical coupling coefficients, $\boldsymbol{\mu}_p^k$ and $\boldsymbol{\mu}_n^k$ the vectors

of hygromechanical coupling coefficients, which in an explicit for are:

$$\boldsymbol{\lambda}_p^k = \left\{ \lambda_1^k \quad \lambda_2^k \quad \lambda_6^k \right\}^T, \quad \boldsymbol{\lambda}_n^k = \left\{ 0 \quad 0 \quad \lambda_3^k \right\}^T \tag{9}$$

$$\boldsymbol{\mu}_p^k = \left\{ \mu_1^k \quad \mu_2^k \quad \mu_6^k \right\}^T, \quad \boldsymbol{\mu}_n^k = \left\{ 0 \quad 0 \quad \mu_3^k \right\}^T \tag{10}$$

The material coefficients C_{ij} depend on the Young, shear, and Poisson moduli, see Reddy's book [35]. The matrix of materials coefficients, as written in Eq. 6, has been already rotated from the material reference system to the global reference system (x, y, z).

Variable kinematics based on Carrera Unified Formulation

In the framework of CUF, the displacement vector $\boldsymbol{u} = \{u, v, w\}$ can be expressed utilizing expansion functions as follows:

$$\begin{cases} u(x,y,z) = F_0(z)u_0(x,y) & +F_1(z)u_1(x,y) & +\cdots+F_N(z)u_N(x,y) \\ v(x,y,z) = F_0(z)v_0(x,y) & +F_1(z)v_1(x,y) & +\cdots+F_N(z)v_N(x,y) \\ w(x,y,z) = F_0(z)w_0(x,y) & +F_1(z)w_1(x,y) & +\cdots+F_N(z)w_N(x,y) \end{cases} \tag{11}$$

In a more compact form, CUF can be expressed in the following form for ESL models:

$$\delta\boldsymbol{u}(x,y,z) = F_\tau(z)\delta\boldsymbol{u}_\tau(x,y); \qquad \boldsymbol{u}(x,y,z) = F_s(z)\boldsymbol{u}_s(x,y) \qquad \tau, s = 0, 1, ..., N \tag{12}$$

CUF-based LW models can be written as:

$$\delta\boldsymbol{u}^k(x,y,\zeta_k) = F_\tau(\zeta_k)\delta\boldsymbol{u}_\tau^k(x,y); \qquad \boldsymbol{u}^k(x,y,\zeta_k) = F_s(\zeta_k)\boldsymbol{u}_s^k(x,y) \qquad \tau, s = 0, 1, ..., N \tag{13}$$

where Ω is the in-plane domain, and $\delta\boldsymbol{u}$ indicates the virtual displacement associated with the virtual work and k is the index of a layer in the laminated plate. $F_\tau^{(k)}$ and $F_s^{(k)}$ are the so called thickness functions whose independent variable is either z defined in the whole thickness domain $z \in [-\frac{h}{2}, \frac{h}{2}]$ for ESL models, or ζ_k defined in each layer domain $\zeta_k \in [-1, 1]$ for LW models. Depending on the type of

expansion functions, N may represent the order of the expansion or the number of expansion terms. $\boldsymbol{u}_s$ represents the unknown primary variables which are the coefficients of corresponding expansion terms, whose independent variables are x and y. τ and s are the indexes of the expansion terms, and the Einstein summation rule is used.

Higher-Order Theories

In the case of Equivalent Single Layer (ESL) models, Taylor series expansions can be employed as thickness functions:

$$\boldsymbol{u} = F_0\,\boldsymbol{u}_0 + F_1\,\boldsymbol{u}_1 + \ldots + F_N\,\boldsymbol{u}_N = F_s\,\boldsymbol{u}_s, \qquad s = 0, 1, \ldots, N \tag{14}$$

$$F_0 = z^0 = 1, \quad F_1 = z^1 = z, \quad \ldots, \quad F_N = z^N \tag{15}$$

Classical models, such as those based on the First-Order Shear Deformation Theory (FSDT) [36, 37], can be obtained with an ESL approach with $N = 1$, by imposing a constant transverse displacement through the thickness via penalty techniques. Also, a model based on the hypotheses of Classical Lamination Theory (CLT) [38] can be expressed employing CUF by applying a penalty technique to the constitutive equations to impose null transverse shear strains.

Refined ESL models based on trigonometric and exponential series

In the framework of ESL models, if trigonometric sine series with a constant term are adopted, the displacement vector can be written as follows:

$$\boldsymbol{u}(x, y, z) = \boldsymbol{u}_0(x, y) + \sin\left(\frac{\pi z}{h}\right)\,\boldsymbol{u}_1(x, y) + ... + \sin\left(\frac{n\pi z}{h}\right)\,\boldsymbol{u}_N(x, y) \tag{16}$$

where h is the thickness of the whole laminated structure and n is the half waves number. If the linear Taylor term is considered, the displacement vector is

$$\boldsymbol{u}(x, y, z) = \boldsymbol{u}_0(x, y) + z\,\boldsymbol{u}_1(x, y) + \sin\left(\frac{\pi z}{h}\right)\,\boldsymbol{u}_2(x, y) + ... + \sin\left(\frac{n\pi z}{h}\right)\,\boldsymbol{u}_{N+1}(x, y) \tag{17}$$

For trigonometric cosine series,

$$\boldsymbol{u}(x,y,z) = \boldsymbol{u}_0(x,y) + \cos\left(\frac{\pi z}{h}\right)\,\boldsymbol{u}_1(x,y) + ... + \cos\left(\frac{n\pi z}{h}\right)\,\boldsymbol{u}_N(x,y) \tag{18}$$

and with the linear term,

$$\boldsymbol{u}(x,y,z) = \boldsymbol{u}_0(x,y) + z\,\boldsymbol{u}_1(x,y) + \cos\left(\frac{\pi z}{h}\right)\,\boldsymbol{u}_2(x,y) + ... + \cos\left(\frac{n\pi z}{h}\right)\,\boldsymbol{u}_{N+1}(x,y) \tag{19}$$

Considering the complete trigonometric series,

$$\begin{aligned}\boldsymbol{u}(x,y,z) = \boldsymbol{u}_0(x,y) + \sin\left(\frac{\pi z}{h}\right)\,\boldsymbol{u}_1(x,y) + \cos\left(\frac{\pi z}{h}\right)\,\boldsymbol{u}_2(x,y) + ... + \sin\left(\frac{n\pi z}{h}\right)\,\boldsymbol{u}_{2N-1}(x,y) + \\ + \cos\left(\frac{n\pi z}{h}\right)\,\boldsymbol{u}_{2N}(x,y)\end{aligned} \tag{20}$$

If the linear contribution is considered,

$$\begin{aligned}\boldsymbol{u}(x,y,z) = \boldsymbol{u}_0(x,y) + z\,\boldsymbol{u}_1(x,y) + \sin\left(\frac{\pi z}{h}\right)\,\boldsymbol{u}_2(x,y) + \cos\left(\frac{\pi z}{h}\right)\,\boldsymbol{u}_3(x,y) + ...+ \\ + \sin\left(\frac{n\pi z}{h}\right)\,\boldsymbol{u}_{2N}(x,y) + \cos\left(\frac{n\pi z}{h}\right)\,\boldsymbol{u}_{2N+1}(x,y)\end{aligned} \tag{21}$$

If exponential series are employed, the displacement field can be expressed as:

$$\boldsymbol{u}(x,y,z) = \boldsymbol{u}_0(x,y) + e^{(z/h)}\,\boldsymbol{u}_1(x,y) + ... + e^{(nz/h)}\,\boldsymbol{u}_N(x,y) \tag{22}$$

and adding the linear term one obtains

$$\boldsymbol{u}(x,y,z) = \boldsymbol{u}_0(x,y) + z\,\boldsymbol{u}_1(x,y) + e^{(z/h)}\,\boldsymbol{u}_2(x,y) + ... + e^{(nz/h)}\,\boldsymbol{u}_{N+1}(x,y) \tag{23}$$

Refined ESL models with Murakami zig-zag function

According to Murakami [39], a zig-zag term can be introduced into Eq. (14) leading to refined ESL zig-zag models,

$$\boldsymbol{u} = \; F_0\,\boldsymbol{u}_0 \; + \; \ldots \; + \; F_N\,\boldsymbol{u}_N \; + \; (-1)^k \zeta_k \boldsymbol{u}_Z. \tag{24}$$

Subscript Z refers to the Murakami zig-zag function. Refined zig-zag models can be obtained by adding the zig-zag term to the Taylor polynomials, trigonometric or exponential series expansions.

Refined LW models based on Legendre polynomials

If Legendre polynomials are adopted, the displacement field defined for a layer k can be expressed as

$$\boldsymbol{u}^k = F_t\, \boldsymbol{u}_t^k + F_b\, \boldsymbol{u}_b^k + F_r\, \boldsymbol{u}_r^k = F_s\, \boldsymbol{u}_s^k, \qquad s = t, b, r\ , \quad r = 2, ..., N. \tag{25}$$

The expansion terms are

$$F_t = \frac{P_0 + P_1}{2}, \quad F_b = \frac{P_0 - P_1}{2}, \quad F_r = P_r - P_{r-2}. \tag{26}$$

P_j is the j^{th}-order Legendre polynomial defined in the ζ_k-domain: $-1 \leq \zeta_k \leq 1$. The displacements on the top (t) and bottom (b) surfaces are used as unknown variables and one can impose the following compatibility conditions at the interfaces:

$$u_t^k = u_b^{k+1}, \qquad k = 1, N_l - 1. \tag{27}$$

The employment of hierarchical Legendre polynomials as basis functions for the development of variable kinematic models was presented by Szab, Dster, and Rank [40]. Other implementations of Legendre polynomials in the framework of CUF can be found in [41–43].

Refined LW models adopting Sampling Surfaces method (SaS)

Kulikov [44–46] proposed the Sampling Surfaces method (SaS) as an LW model based on Lagrange interpolation polynomials. Within each layer, an arbitrary number of sampling surfaces parallel to the middle surface are introduced. Each SaS is located at a Lagrange interpolation point, and the displacements at these points are taken as primary unknowns. The present work implements the SaS technique for the plate element based on CUF. In SaS, the displacement field can be defined as

$$\boldsymbol{u}^k = F_0\, \boldsymbol{u}_0^k + F_1\, \boldsymbol{u}_1^k + \ldots + F_N\, \boldsymbol{u}_N^k = F_s\, \boldsymbol{u}_s^k, \qquad s = 0, 1, \ldots, N. \tag{28}$$

$F_s(\zeta_k)$ (thickness function) is a Lagrange polynomial of order N,

$$F_s(\zeta_k) = \prod_{i=0, i\neq s}^{N} \frac{\zeta_k - \zeta_{k_i}}{\zeta_{k_s} - \zeta_{k_i}} \tag{29}$$

ζ_{k_s} are located at the prescribed interpolation points. $\zeta_{k_0} = -1$ and $\zeta_{k_N} = 1$ correspond to the top and bottom positions of the k^{th} layer, respectively.

Through-the-thickness variation of temperature and moisture concentration

The temperature variation through the thickness can be obtained by solving Fourier heat conduction equation as described in [7] for multilayered plates. If the temperature on the top and bottom surfaces are given, a priori assumed linear temperature variation profile through-the -thickness can be obtained as follows:

$$\theta(z) = \theta_b + \frac{\theta_t - \theta_b}{h} \cdot (z + \frac{h}{2}) \quad z \in [-\frac{h}{2}, \frac{h}{2}] \tag{30}$$

where the subscripts b and t refer to the bottom and top surfaces, respectively. It is evident that the temperature continuity between two layers can be naturally guaranteed in this manner. Similarly, an assumed linear moisture concentration profile could be described as:

$$\eta(z) = \eta_b + \frac{\eta_t - \eta_b}{h} \cdot (z + \frac{h}{2}) \quad z \in [-\frac{h}{2}, \frac{h}{2}] \tag{31}$$

Alternatively, a more physically meaningful profile can be obtained by solving Fourier heat conduction equation for temperature variation, or the Fick law for moisture concentration distribution. In multilayered plate structures, for the k^{th} homogeneous orthotropic layer, the Fourier differential equation for heat conduction problems reads:

$$K_1^k \frac{\partial^2 \theta}{\partial x^2} + K_2^k \frac{\partial^2 \theta}{\partial y^2} + K_3^k \frac{\partial^2 \theta}{\partial z^2} = 0 \tag{32}$$

where K_1^k, K_2^k and K_3^k are the thermal conduction coefficients in material coordinates (1,2,3) for the k^{th} layer and will be rotated to the general reference system (x, y, z). In the k^{th} layer, K_1^k, K_2^k and K_3^k are assumed to be constants. The relationship between the temperature θ and the transverse normal

heat flux q_z is described by

$$q_z^k = K_3^k \frac{\partial \theta}{\partial z} \tag{33}$$

For multilayered structures, continuity conditions of θ and q_z holds in the thickness direction at each layer interface, reading:

$$\theta_t^k = \theta_b^{k+1}, \quad q_{zt}^k = q_{zb}^{k+1} \qquad k = 1, \cdots, N_l - 1 \tag{34}$$

where N_l is the number of layers in the composite laminate. In this work, the governing equation and boundary conditions are satisfied in each layer by assuming the following temperature field:

$$\theta(x, y, z) = \theta_A(z) \cdot \theta_\Omega(x, y) \tag{35}$$

where, for the cases studied in this paper, θ_Ω has a bisinusoidal form as follows:

$$\theta_\Omega(x, y) = \sin(\frac{m\pi x}{a}) \cdot \sin(\frac{n\pi y}{b}) \tag{36}$$

For the solution of the Fourier heat conduction equation, the reader can refer to the authors' previous works [29, 47, 48]. Calculated moisture concentration profiles can be acquired by solving the Fick law, which postulates that the flux J goes from regions of high concentration to areas of low concentration, with a diffusion rate that is proportional to the concentration gradients (spatial derivatives). For a steady state plate structure, the Fick second law can be expressed as

$$D_1^k \frac{\partial^2 \eta}{\partial x^2} + D_2^k \frac{\partial^2 \eta}{\partial y^2} + D_3^k \frac{\partial^2 \eta}{\partial z^2} = 0 \tag{37}$$

where D_1^k, D_2^k and D_3^3 are the diffusion coefficients (diffusivity) and η is the moisture concentration. Accordingly, moisture concentration η and diffusion flux through the thickness J_z can be related by

$$J_z^k = D_3^k \frac{\partial \eta}{\partial z} \tag{38}$$

and the continuity of η and J_z at layer interfaces can be imposed as

$$\eta_t^k = \eta_b^{k+1}, \quad J_{zt}^k = J_{zb}^{k+1} \qquad k = 1, \cdots, N_l - 1 \tag{39}$$

Similarly to the thermal case, the 3D hygroscopic field can be described as

$$\eta(x, y, z) = \eta_A(z) \cdot \eta_\Omega(x, y) \tag{40}$$

If a bisinusoidal load is imposed,

$$\eta_\Omega(x, y) = \sin(\frac{m\pi x}{a}) \cdot \sin(\frac{n\pi y}{b}) \tag{41}$$

As discussed above, the Fick law can be solved in analogy with the Fourier heat conduction equation under given hygroscopic boundary conditions on the top and bottom surfaces of the laminated structures.

MITC9 finite element and governing equations

This section presents the derivation of the finite element stiffness matrix based on the Principle of Virtual Displacement (PVD) in the case of multilayered plates under hygrothermal environmental load. A nine-node element adopting the Mixed Interpolation of Tensorial Component (MITC) method is formulated in the framework of CUF. The displacement vector interpolated on the element nodes utilizing Lagrangian shape functions N_i reads

$$\delta \boldsymbol{u}_\tau = N_i \delta \boldsymbol{U}_{\tau_i}, \qquad \boldsymbol{u}_s = N_j \boldsymbol{U}_{s_j} \qquad i, j = 1, \cdots, 9 \tag{42}$$

$\boldsymbol{U}_{s_j}$ and $\delta \boldsymbol{U}_{\tau_i}$ are the nodal displacement vector and its virtual variation, respectively. Therefore, the strain expression (Eq. (3)) becomes

$$\begin{cases} \boldsymbol{\epsilon}_p = F_s \boldsymbol{D}_p N_j \boldsymbol{U}_{s_j} \\ \boldsymbol{\epsilon}_n = F_s \boldsymbol{D}_{n\Omega} N_j \boldsymbol{U}_{s_j} + F_{s,_z} N_j \boldsymbol{U}_{s_j} \end{cases} \tag{43}$$

To contrast the shear locking of thin plates, a specific interpolation strategy according to MITC method is used to derive the strain components on the nine-node element, and the corresponding interpolation points (*tying points*) are illustrated in previous authors' works related to the use of the MITC9 element based on the CUF [49–52].

Considering the constitutive equations (Eq. (5)) and the strain vectors (Eq. (43)), scalar temperature

field θ as well as moisture concentration field η, by applying PVD, one obtains the expression of the internal work for partially coupled hygrothermal problems:

$$\delta L_{int} = \int_{\Omega}\int_{A_k} \delta {\boldsymbol{\epsilon}^k}^T \boldsymbol{\sigma}^k d\Omega dz = \int_{\Omega}\int_{A_k} [\delta {\boldsymbol{\epsilon}_p^k}^T (\boldsymbol{\sigma}_{pu}^k - \boldsymbol{\sigma}_{p\theta}^k - \boldsymbol{\sigma}_{p\eta}^k) + \delta {\boldsymbol{\epsilon}_n^k}^T (\boldsymbol{\sigma}_{nu}^k - \boldsymbol{\sigma}_{n\theta}^k - \boldsymbol{\sigma}_{n\eta}^k)] d\Omega dz \quad = \delta L_{ext} \tag{44}$$

where A_k is the thickness domain of layer k of the plate. δL_{int} represents the variation of the internal work, while δL_{ext} is the external work. Noting that in this work no mechanical loads are considered, which means that $\delta L_{ext} = 0$, and the internal work δL_{int} is caused purely by the mechanical expansion related to temperature rise and moisture absorption, thus the following expression can be obtained:

$$\int_{\Omega}\int_{A_k} (\delta {\boldsymbol{\epsilon}_p^k}^T \boldsymbol{\sigma}_{pu}^k + \delta {\boldsymbol{\epsilon}_n^k}^T \boldsymbol{\sigma}_{nu}^k) d\Omega dz \quad = \int_{\Omega}\int_{A_k} (\delta {\boldsymbol{\epsilon}_p^k}^T \boldsymbol{\sigma}_{p\theta}^k + \delta {\boldsymbol{\epsilon}_n^k}^T \boldsymbol{\sigma}_{n\theta}^k) d\Omega dz + \int_{\Omega}\int_{A_k} (\delta {\boldsymbol{\epsilon}_p^k}^T \boldsymbol{\sigma}_{p\eta}^k + \delta {\boldsymbol{\epsilon}_n^k}^T \boldsymbol{\sigma}_{n\eta}^k) d\Omega dz \tag{45}$$

By substituting the constitutive equations (Eq. (5)), the geometrical relations (Eq. (43)) after the application of MITC method, the displacement expression (Eqs. (12) and (13)) and the FEM discretization (Eq. (42)), the following governing equations can be obtained:

$$\delta \boldsymbol{U}_{\tau_i}^k : \quad \boldsymbol{K}_{uu}^{k\tau sij} \boldsymbol{U}_{s_j}^k = \boldsymbol{\Theta}^{k\tau_i} + \boldsymbol{H}^{k\tau_i} \tag{46}$$

The 3×3 matrix $\boldsymbol{K}_{uu}^{k\tau sij}$ is the fundamental mechanical nucleus, which is the core unit of the stiffness matrix according to CUF, and its explicit expression is given in [53] for shells (plate is a particular case of shell for radii of curvature tending to infinite). The stiffness matrix of the structure can be obtained by applying the Einstein summation rule, then assembling the fundamental nucleus at laminate level in the framework of either ESL or LW models and at element level considering the nodes. Finally, the global stiffness matrix is assembled using the connectivity matrix. $\boldsymbol{\Theta}^{k\tau_i}$ and $\boldsymbol{H}^{k\tau_i}$ are the equivalent thermal and hygroscopic load vectors, and their explicit expressions are given in Eq. (47) and Eq. (48), respectively:

$$\boldsymbol{\Theta}^{k\tau_i} = \begin{Bmatrix} \Theta_x^{k\tau i} \\ \Theta_y^{k\tau i} \\ \Theta_z^{k\tau i} \end{Bmatrix} = \begin{Bmatrix} \lambda_6^k J^{\theta k\tau} W_{i,y}^{\theta} + \lambda_1^k J^{\theta k\tau} W_{i,x}^{\theta} \\ \lambda_2^k J^{\theta k\tau} W_{i,y}^{\theta} + \lambda_6^k J^{\theta k\tau} W_{i,x}^{\theta} \\ \lambda_3^k J^{\theta k\tau,z} W_i^{\theta} \end{Bmatrix} \tag{47}$$

$$\boldsymbol{H}^{k\tau_i} = \left\{ \begin{array}{l} H_x^{k\tau i} \\ H_y^{k\tau i} \\ H_z^{k\tau i} \end{array} \right\} = \left\{ \begin{array}{l} \mu_6^k J^{\eta k\tau} W_{i,y}^{\eta} + \mu_1^k J^{\eta k\tau} W_{i,x}^{\eta} \\ \mu_2^k J^{\eta k\tau} W_{i,y}^{\eta} + \mu_6^k J^{\eta k\tau} W_{i,x}^{\eta} \\ \mu_3^k J^{\eta k\tau,z} W_i^{\eta} \end{array} \right\} \tag{48}$$

$W_i, W_{i,x}, W_{i,y}$ are the integrals in the in-plane domain Ω and $J^{k\tau}$ and $J^{k\tau,z}$ are the integrals defined within the through-the-thickness domain A_k of the layer,

$$W_i^{\theta} = \int_{\Omega} N_i \theta_{\Omega}\, dxdy, \quad W_{i,x}^{\theta} = \int_{\Omega} \frac{\partial N_i}{\partial x} \theta_{\Omega}\, dxdy, \quad W_{i,y}^{\theta} = \int_{\Omega} \frac{\partial N_i}{\partial y} \theta_{\Omega}\, dxdy \tag{49}$$

$$J^{\theta k\tau} = \int_{A_k} F_{\tau} \theta_k dz, \quad J^{\theta k\tau,z} = \int_{A_k} \frac{\partial F_{\tau}}{\partial z} \theta_k dz \tag{50}$$

$$W_i^{\eta} = \int_{\Omega} N_i \eta_{\Omega}\, dxdy, \quad W_{i,x}^{\eta} = \int_{\Omega} \frac{\partial N_i}{\partial x} \eta_{\Omega}\, dxdy, \quad W_{i,y}^{\eta} = \int_{\Omega} \frac{\partial N_i}{\partial y} \eta_{\Omega}\, dxdy \tag{51}$$

$$J^{\eta k\tau} = \int_{A_k} F_{\tau} \eta_k dz, \quad J^{\eta k\tau,z} = \int_{A_k} \frac{\partial F_{\tau}}{\partial z} \eta_k dz \tag{52}$$

θ and η denote thermal and hygroscopic cases, respectively. F_{τ} refers to a general expansion term in the displacement field according to CUF, and N_i represents the shape function corresponding to node i in the finite element. For more details, the reader can refer to [26, 29, 53].

Results

The numerical analysis of this work focuses on investigating the capability of a variety of models with variable kinematics in the analysis of cross-ply symmetrically laminated multilayered structures under hygrothermal environmental loads. This section consists of two numerical cases:

- A three-layer (0°/90°/0°) square plate under thermal load;
- A three-layer (0°/90°/0°) square plate under hygroscopic load.

Acronyms are used to indicate the various models used. For ESL, Table 1 shows all the cases used in this paper.

For example, "ES2C2" and "ET1Exp2Z" refer to the following expansions,

$$\boldsymbol{u}^k(x,y,z) = \boldsymbol{u}_0^k(x,y) + \sin(\frac{\pi z}{h})\boldsymbol{u}_1^k(x,y) + \cos(\frac{\pi z}{h})\boldsymbol{u}_2^k(x,y) + \sin(\frac{2\pi z}{h})\boldsymbol{u}_3^k(x,y) + \cos(\frac{2\pi z}{h})\boldsymbol{u}_4^k(x,y) \quad (53)$$

$$\boldsymbol{u}^k(x,y,z) = \boldsymbol{u}_0^k(x,y) + z\boldsymbol{u}_1^k(x,y) + e^{\frac{z}{h}}\boldsymbol{u}_2^k(x,y) + e^{\frac{2z}{h}}\boldsymbol{u}_3^k(x,y) + (-1)^k\zeta_k\boldsymbol{u}_{4_Z}^k \quad (54)$$

The subscript a denotes the adoption of assumed linear temperature or moisture concentration profiles, whereas c indicates that through-the-thickness distributions are calculated by via Fourier or Fick laws. LW models are indicated as follows:

- "SaSn" indicates a Sampling Surfaces model with n interpolation points.
- "LGDn" indicates a model adopting Legendre polynomials up to the n^{th} order.

Analytical solutions are used in some cases and obtained via the Navier method. In the following tables, N_{exp} is indicated and represents the expansion terms of the model.

Square orthotropic symmetrically laminated plates under thermal load

Bending of a simply supported cross-ply square composite plate under thermal load is analyzed. The reference solutions were proposed by Bhaskar et al. [54], in which thermal analysis was carried out with assumed linear temperature profiles. The composite square plates analyzed have three layers with lamination sequence of (0°/90°/0°). The 3D temperature field is given by

$$\theta(x,y,z) = \theta_A(z)\cdot\sin(\frac{m\pi x}{a})\sin(\frac{n\pi y}{b}) \quad (55)$$

with bisinusoidal in-plane distribution ($m = n = 1$). The temperature variation through the thickness is depicted with $\theta_A(z)$, and the thermal boundary conditions are assumed to be $\hat{\theta}_A(\frac{h}{2}) = 1\text{K}$, $\hat{\theta}_A(-\frac{h}{2}) =$ -1K. The physical properties of the composite lamina are given in Table 2, in which L and T refer to the direction parallel and perpendicular to the fiber direction, respectively. The geometrical dimensions are $a = b = 1$, laminates with $a/h = 2$, 10 and 100 were studied, and the three layers have the same thickness. Deflections and stresses are adimensionalized as,

$$\bar{u}_z = \frac{w}{h\alpha_L\theta_A S^2}, \quad \bar{\sigma}_{ii} = \frac{\sigma_{ii}}{E_T\alpha_L\theta_A}, \quad \bar{\sigma}_{ij} = \frac{\sigma_{ij}}{E_T\alpha_L\theta_A}, \quad S = a/h \quad (56)$$

where $i, j = x, y, z$.

First, a mesh convergence study was considered with LGD4, $a/h = 100$, and an assumed linear temperature profile. According to the results shown in Table 3, a mesh of 10×10 is sufficient to ensure the convergence of FEM solution with satisfactory accuracy. The results also show that the adopted MITC9 element is locking free for thin plates.

LW models were considered first. Table 4 presents the obtained displacement and stress values. Moreover, N_{exp} indicates the number of expansion terms of each model. The calculated temperature variation through the thickness is in Fig. 2. Stress distributions through the thickness are given in Fig. 3. The influence of the expansion terms is shown in Table 4. The results suggest that:

- A perfect match with [54] is found.
- As known, an assumed linear variation of temperature through the thickness leads to satisfactory results in the case of a thin plate. On the other hand, such an assumed profile should not be used for thick plates.

Various ESL models were then investigated with calculated temperature variation profiles. ETn models were first assessed as in Table 5. Since FSDT is not a complete linear case, its number of expansion terms was denoted as "2*". It can be stated that:

- For thick plates, nine expansion terms are necessary, while for moderate thick and thin plates, six terms are enough.
- Compared with the computational costs of LGD4 and SaS5, the present ESL kinematics are more efficient for moderate thick and thin plates.
- More often than not, FSDT failed to provide proper displacement and stress evaluations.

ESL models with exponential expansions are considered in Table 6. It can be observed that:

- Stress results are less accurate than the previous cases.
- The addition of the linear Taylor term gives some improvements, but still unsatisfactory accuracies were obtained.

Table 7 show the results from ESL trigonometric expansions. The results show that:

- For thick plates, σ_{xz} requires ES5C5Z or ET1S3C3Z. However, the latter is preferable due to fewer expansion terms required.
- For moderately thick and thin plates, ESnCnZ can provide desired approximations but are more cumbersome than ETnZ. The addition of a first-order Taylor term, i.e. using ET1SnCnZ, the results improve to a great extend. In particular, ET1S1C1Z gives good accuracy.

Models shown above, are compared in Fig. 4. The transverse shear stress $\bar{\sigma}_{xz}$ is considered for different thickness ratios. It can be found that:

- The use of SaS5 (as well as LGD4) is recommended to capture the transverse shear stress distribution through the thickness.
- As known, the Murakami zig-zag function can improve the transverse shear stress distribution in ESL models.
- Stress distributions obtained with exponential theories are less accurate than the previous cases.
- For thick plates, σ_{xz} requires the addition of the linear Taylor term, when trigonometric expansions are used.

In general, the results obtained have demonstrated that ETnZ and ET1SnCnZ models perform extremely well. Based on the study above, ETnZ and ET1SnCnZ are chosen for the hygrothermal analysis in the following study cases.

Square orthotropic symmetrically laminated plates under hygroscopic load

Square cross-ply laminated plates with stacking sequence (0°/90°/0°) subjected to hygroscopic loads are analyzed. The dimensions are $a = b = 0.1m$, $a/h = 2, a/h = 10$, and $a/h = 100$. The mechanical and hygroscopic properties of the lamina are listed in Table 8 and Table 9, respectively. Moisture expansion coefficients β_{11}, β_{22}, and β_{33} were retrieved from [55]. Moisture diffusion coefficients D_{11}, D_{22}, and D_{33} were chosen and set under temperature 300 K as in [13]. Hygroscopic loads are defined as:

$$\eta(x, y, z) = \eta_A(z) \cdot \sin(\frac{m\pi x}{a}) \sin(\frac{n\pi y}{b}) \tag{57}$$

where $\eta_A(z)$ describes the moisture concentration profile, $m = n = 1$, and the moisture concentration conditions are $\eta_A(-\frac{h}{2}) = 0$ and $\eta_A(\frac{h}{2}) = 1\%$.

LW models were considered first. Moisture concentration profiles are shown in Fig. 5. Displacement and stress distributions are presented in Fig. 6, in which for the convenience of illustration, the stresses are amplified by 50 times in the plots when necessary, denoted by "$*50$". Table 10 summarizes the displacement and stress evaluation on a specific set of monitoring points. The results show that:

- LW models provide highly accurate results.
- As seen in the thermal case, for moderately thick and thin plates, linear profiles are enough. On the other hand, thick plates require calculated profiles.

ETnZ and ET1SnCnZ were then considered, as shown in Fig. 7. The results suggest that, in the case of hygroscopic loads, these models are less accurate than in the case of thermal loads, and LW should be preferred.

Conclusions

In the framework of the Carrera Unified Formulation, it is possible to integrate various and miscellaneous approximation theories to obtain refined and advanced models with various kinematics and an arbitrary number of expansion terms for the analysis of multilayered structures. In this paper, steady state mechanical responses of composite plates under thermal/hygroscopic loads are studied with CUF-based variable kinematics adopting LW and ESL approaches, respectively. A MITC9 element is employed to guarantee locking free FEM analysis. Both assumed linear temperature/moisture concentration profiles through the thickness, and calculated variations (by solving the diffusion law) are considered. The analogy between heat conduction and moisture diffusion plays a key role when extending the analysis methodology of thermoelastic problems to hygrothermal ones. Hygrothermal analysis has been carried out on multilayered composite plates. Transverse displacement and stresses are reported for various aspect ratios. The convergence rates of various kinematics are compared. Based on the above work, some conclusions can be drawn as:

1. With a sufficient number of expansion terms, most of the kinematics studied can achieve a good approximation of displacements and stresses with satisfactory accuracy, even for thick plates, and

the expansion number needed depends on the cases studied.

2. For laminates with various aspect ratios, the numbers of expansion terms necessary to obtain converged numerical results are usually different, and thick laminates need more expansion terms.

3. When applied to hygrothermal analysis, classical theory FSDT gives incorrect results even for thin laminates.

4. For thin laminates, linear variation of temperature/moisture concentration through the thickness is a sufficient assumption, whereas for thick layered plates this assumption can lead to over estimated stress evaluation compared with results using profiles obtained by solving Fourier heat conduction equation or Fick Law.

5. For the hygrothermal cases studied, LW models employing Legendre polynomials of the fourth-order (LGD4) and the Sampling Surfaces method with five interpolation nodes (SaS5) can guarantee continuous transverse shear stress distribution through the thickness for composite laminates with a broad range of length to thickness ratios (from 2 to 500).

6. Variable ESL kinematics ETnZ and ET1SnCnZ have been tested. It has been demonstrated that when a sufficient number of expansion terms are used, with the help of the Murakami zig-zag function, ETnZ, and ET1SnCnZ are capable of capturing transverse shear stress distribution through the thickness of the three-layer plates under symmetrical load. In some cases, these two classes of ESL kinematics can be more computationally efficient than LW models with comparable accuracy. However, for the three-layer plates under unsymmetrical load, ESL models are less efficient in capturing the zig-zag effects.

7. Compared with ESL models, LW models can provide results with better accuracy in approximating the through the thickness distribution of transverse shear stresses in composite laminates.

A companion work to this one is devoted to the modelling of doubly-curved composite shells with antisymmetric lamination subjected to hygrothermal loads. In that paper, very similar conclusions about the accuracy of the models used are drawn.

Future works should be devoted to the axiomatic/asymptotic analysis of the influence of each term and the definition of Best Theory Diagrams, as in [56].

Acknowledgment

This research work has been carried out within the project FULLCOMP (FULLy analysis, design, manufacturing, and health monitoring of COMPosite structures), funded by the European Union Horizon 2020 Research and Innovation program under the Marie Skłodowska Curie grant agreement No. 642121. E. Carrera has been partially supported by the Russian Science Foundation (Grant No. 15-19-30002).

References

[1] R. B. Pipes, J. R. Vinson, and T. W. Chou, "On the hygrothermal response of laminated composite systems," *Journal of Composite Materials*, vol. 10, no. 2, pp. 129–148, 1976.

[2] G. C. Sih, J. Michopoulos, and S. C. Chou, *Hygrothermoelasticity*. Springer Science & Business Media, Dec. 2012.

[3] T. Kant and R. Khare, "Finite element thermal stress analysis of composite laminates using a higher-order theory," *Journal of Thermal Stresses*, vol. 17, no. 2, pp. 229–255, 1994.

[4] A. Khdeir and J. Reddy, "Thermal stresses and deflections of cross-ply laminated plates using refined plate theories," *Journal of Thermal Stresses*, vol. 14, no. 4, pp. 419–438, 1991.

[5] E. Carrera, "An assessment of mixed and classical theories for the thermal stress analysis of orthotropic multilayered plates," *Journal of Thermal Stresses*, vol. 23, no. 9, pp. 797–831, 2000.

[6] A. Robaldo and E. Carrera, "Mixed finite elements for thermoelastic analysis of multilayered anisotropic plates," *Journal of Thermal Stresses*, vol. 30, no. 2, pp. 165–194, 2007.

[7] V. Tungikar and K. M. Rao, "Three dimensional exact solution of thermal stresses in rectangular composite laminate," *Composite Structures*, vol. 27, no. 4, pp. 419–430, 1994.

[8] E. Carrera, "Temperature profile influence on layered plates response considering classical and advanced theories," *AIAA Journal*, vol. 40, no. 9, pp. 1885–1896, 2002.

[9] P. Nali, E. Carrera, and A. Calvi, "Advanced fully coupled thermo-mechanical plate elements for multilayered structures subjected to mechanical and thermal loading," *International Journal for Numerical Methods in Engineering*, vol. 85, no. 7, pp. 896–919, 2011.

[10] J. Fourier, *Theorie analytique de la chaleur, par M. Fourier.* Chez Firmin Didot, père et fils, 1822.

[11] A. Fick, "On liquid diffusion," *Journal of Membrane Science*, vol. 100, no. 1, pp. 33–38, 1995.

[12] C. H. Shen and G. S. Springer, "Moisture absorption and desorption of composite materials," *Journal of Composite Materials*, vol. 10, no. 1, pp. 2–20, 1976.

[13] S. W. Tsai and T. N. Massard, *Composites design.* Think Composites, 1988.

[14] A. Szekeres and J. Engelbrecht, "Coupled thermal and moisture fields with application to composites," *Periodica Polytechnica. Engineering. Mechanical Engineering*, vol. 41, no. 2, p. 151, 1997.

[15] A. Szekeres, "Analogy between heat and moisture: Thermo-hygro-mechanical tailoring of composites by taking into account the second sound phenomenon," *Computers & Structures*, vol. 76, no. 1, pp. 145–152, 2000.

[16] A. Benkeddad, M. Grediac, and A. Vautrin, "On the transient hygroscopic stresses in laminated composite plates," *Composite Structures*, vol. 30, no. 2, pp. 201–215, 1995.

[17] A. Benkeddad, M. Grediac, and A. Vautrin, "Computation of transient hygroscopic stresses in laminated composite plates," *Composites Science and Technology*, vol. 56, no. 7, pp. 869–876, 1996.

[18] A. Tounsi, M. Bouazza, and E. A. Bedia, "Computation of transient hygroscopic stresses in unidirectional laminated composite plates with cyclic and asymmetrical environmental conditions," *International Journal of Mechanics and Materials in Design*, vol. 1, no. 3, pp. 271–286, 2004.

[19] A. Tounsi and E. A. Bedia, "Simplified method for prediction of transient hygroscopic stresses in polymer matrix composites with symmetric environmental conditions," *Applied Composite Materials*, vol. 10, no. 1, pp. 1–18, 2003.

[20] A. Tounsi and E. A. Bedia, "Some observations on the evolution of transversal hygroscopic stresses in laminated composites plates: effect of anisotropy," *Composite Structures*, vol. 59, no. 4, pp. 445–454, 2003.

[21] A. Tounsi, E. A. Bedia, and A. Benachour, "A new computational method for prediction of transient hygroscopic stresses during moisture desorption in laminated composite plates with different

degrees of anisotropy," *Journal of Thermoplastic Composite Materials*, vol. 18, no. 1, pp. 37–58, 2005.

[22] E. A. Bedia, W. Han, and G. Verchery, "An asymptotic characterisation of the moisture diffusion in polymer matrix composites with cyclic environmental conditions," *Composite Structures*, vol. 49, no. 3, pp. 269–274, 2000.

[23] B. Boukhoulda, E. A. Bedia, and K. Madani, "The effect of fiber orientation angle in composite materials on moisture absorption and material degradation after hygrothermal ageing," *Composite Structures*, vol. 74, no. 4, pp. 406–418, 2006.

[24] B. Patel, M. Ganapathi, and D. Makhecha, "Hygrothermal effects on the structural behaviour of thick composite laminates using higher-order theory," *Composite Structures*, vol. 56, no. 1, pp. 25–34, 2002.

[25] S. Lo, W. Zhen, Y. Cheung, and C. Wanji, "Hygrothermal effects on multilayered composite plates using a refined higher order theory," *Composite Structures*, vol. 92, no. 3, pp. 633–646, 2010.

[26] E. Carrera, "Theories and finite elements for multilayered, anisotropic, composite plates and shells," *Archives of Computational Methods in Engineering*, vol. 9, no. 2, pp. 87–140, 2002.

[27] E. Carrera, "Theories and finite elements for multilayered plates and shells: a unified compact formulation with numerical assessment and benchmarking," *Archives of Computational Methods in Engineering*, vol. 10, no. 3, pp. 215–296, 2003.

[28] E. Carrera, M. Cinefra, and F. A. Fazzolari, "Some results on thermal stress of layered plates and shells by using Unified Formulation," *Journal of Thermal Stresses*, vol. 36, no. 6, pp. 589–625, 2013.

[29] M. Cinefra, S. Valvano, and E. Carrera, "Heat conduction and thermal stress analysis of laminated composites by a variable kinematic MITC9 shell element," *Curved and Layered Structures*, vol. 2, no. 1, pp. 301–320, 2015.

[30] K. J. Bathe, P. S. Lee, and J. F. Hiller, "Towards improving the MITC9 shell element," *Computers & Structures*, vol. 81, no. 8, pp. 477–489, 2003.

[31] C. Chinosi and L. Della Croce, "Mixed-interpolated elements for thin shells," *Communications in Numerical Methods in Engineering*, vol. 14, no. 12, pp. 1155–1170, 1998.

[32] H. C. Huang, "Membrane locking and assumed strain shell elements," *Computers & Structures*, vol. 27, no. 5, pp. 671–677, 1987.

[33] P. Panasz and K. Wisniewski, "Nine-node shell elements with 6 dofs/node based on two-level approximations. part i: Theory and linear tests," *Finite Elements in Analysis and Design*, vol. 44, no. 12, pp. 784–796, 2008.

[34] E. Carrera, M. Cinefra, G. Li, and G. Kulikov, "MITC9 shell finite elements with miscellaneous through-the-thickness functions for the analysis of laminated structures," *Composite Structures*, vol. 154, pp. 360–373, 2016.

[35] J. Reddy, *Mechanics of laminated composite plates and shells. Theory and Analysis*. CRC Press, 2^{nd} ed., 2004.

[36] E. Reissner, "The effect of transverse shear deformation on the bending of elastic plates," *Journal of Applied Mechanics*, vol. 12, no. 2, pp. 69–77, 1945.

[37] R. D. Mindlin, "Influence of rotatory inertia and shear on flexural motions of isotropic, elastic plates," *ASME Journal of Applied Mechanics*, vol. 18, pp. 31–38, 1951.

[38] G. Kirchhoff, "Über das gleichgewicht und die bewegung einer elastishen scheibe," *Journal für die reine und angewandte Mathematik*, vol. 40, pp. 51–88, 1850.

[39] H. Murakami, "Laminated composite plate theory with improved in-plane responses," *Journal of Applied Mechanics*, vol. 53, no. 3, pp. 661–666, 1986.

[40] I. Babuska, B. A. Szabo, and I. N. Katz, "The p-version of the finite element method," *SIAM Journal on Numerical Analysis*, vol. 18, no. 3, pp. 515–545, 1981.

[41] A. Pagani, A. de Miguel, M. Petrolo, and E. Carrera, "Analysis of laminated beams via Unified Formulation and Legendre polynomial expansions," *Composite Structures*, vol. 156, pp. 78 – 92, 2016.

[42] L. Demasi, "Mixed plate theories based on the Generalized Unified Formulation.: Part ii: Layerwise theories," *Composite Structures*, vol. 87, no. 1, pp. 12 – 22, 2009.

[43] E. Carrera and G. Giunta, "Hierarchical evaluation of failure parameters in composite plates," *AIAA Journal*, vol. 47, no. 3, pp. 692–702, 2009.

[44] G. Kulikov and S. Plotnikova, "Exact 3D stress analysis of laminated composite plates by sampling surfaces method," *Composite Structures*, vol. 94, no. 12, pp. 3654–3663, 2012.

[45] G. Kulikov and S. Plotnikova, "Advanced formulation for laminated composite shells: 3D stress analysis and rigid-body motions," *Composite Structures*, vol. 95, pp. 236–246, 2013.

[46] G. Kulikov and S. Plotnikova, "Hybrid-mixed ans finite elements for stress analysis of laminated composite structures: Sampling surfaces plate formulation," *Computer Methods in Applied Mechanics and Engineering*, vol. 303, pp. 374–399, 2016.

[47] M. Cinefra, S. Valvano, and E. Carrera, "Thermal stress analysis of laminated structures by a variable kinematic MITC9 shell element," *Journal of Thermal Stresses*, vol. 39, no. 2, pp. 121–141, 2016.

[48] E. Carrera, F. Fazzolari, and M. Cinefra, *Thermal Stress Analysis of Composite Beams, Plates and Shells*. Elsevier, 2015.

[49] M. Cinefra, E. Carrera, L. Della Croce, and C. Chinosi, "Refined shell elements for the analysis of functionally graded structures," *Composite Structures*, vol. 94, pp. 415–422, 2012.

[50] M. Cinefra, C. Chinosi, and L. Della Croce, "Mitc9 shell elements based on refined theories for the analysis of isotropic cylindrical structures," *Mechanics of Advanced Materials and Structures*, vol. 20, pp. 91–100, 2013.

[51] M. Cinefra and E. Carrera, "Shell finite elements with different through-the-thickness kinematics for the linear analysis of cylindrical multilayered structures," *International Journal for Numerical Methods in Engineering*, vol. 93, pp. 160–182, 2013.

[52] M. Cinefra, "Free-vibration analysis of laminated shells via refined mitc9 elements," *Mechanics of Advanced Materials and Structures*, vol. 23, no. 9, pp. 937–947, 2016.

[53] M. Cinefra and S. Valvano, "A variable kinematic doubly-curved MITC9 shell element for the analysis of laminated composites," *Mechanics of Advanced Materials and Structures*, vol. 23, no. 11, pp. 1312–1325, 2016.

[54] K. Bhaskar, T. Varadan, and J. Ali, "Thermoelastic solutions for orthotropic and anisotropic composite laminates," *Composites Part B: Engineering*, vol. 27, no. 5, pp. 415–420, 1996.

[55] F. Jacquemin and A. Vautrin, "A closed-form solution for the internal stresses in thick composite cylinders induced by cyclical environmental conditions," *Composite Structures*, vol. 58, no. 1, pp. 1–9, 2002.

[56] E. Carrera, M. Cinefra, M. Petrolo, and A. Lamberti, "Best theory diagrams for multilayered plates considering multifield analysis," *Journal of Intelligent Material Systems and Structures*, vol. In Press.

Table 1: Expansion terms of the ESL models.

	z^0	$z^1 \rightarrow z^N$	$(-1)^k\zeta_k$	$\sin\left(\frac{z\pi}{h}\right) \rightarrow \sin\left(\frac{nz\pi}{h}\right)$	$\cos\left(\frac{z\pi}{h}\right) \rightarrow \cos\left(\frac{nz\pi}{h}\right)$	$e^{(z/h)} \rightarrow e^{(nz/h)}$
ETn	√	√	×	×	×	×
ETnZ	√	√	√	×	×	×
ESn	√	×	×	√	×	×
ESnZ	√	×	√	√	×	×
ECn	√	×	×	×	√	×
ECnZ	√	×	√	×	√	×
ESnCn	√	×	×	√	√	×
ESnCnZ	√	×	√	√	√	×
ETnSnCn	√	√	×	√	√	×
ETnSnCnZ	√	√	√	√	√	×
EEXPn	√	×	×	×	×	√
EEXPnZ	√	×	√	×	×	√
ETnEXPn	√	√	×	×	×	√
ETnEXPnZ	√	√	√	×	×	√

Table 2: Assumed mechanical/thermal properties of the lamina [54].

E_L/E_T	G_{LT}/E_T	G_{LT}/E_T	ν_{LT}/ν_{TT}	α_T/α_L	K_L/K_T
25	0.5	0.2	0.25	1125	36.42/0.96

Table 3: Mesh convergence study, displacement and stress evaluation, LGD4, composite plates with $a/h = 100$ subjected to thermal load. Assumed linear temperature profiles are used.

$^a/_h$	Mesh	$\bar{w}$	$\bar{\sigma}_{xx}$	$\bar{\sigma}_{xz}$
		$(\frac{a}{2}, \frac{b}{2}, \frac{h}{2})$	$(\frac{a}{2}, \frac{b}{2}, \frac{h}{2})$	$(0, \frac{b}{2}, \frac{h}{6})$
100	4×4	10.26	981.7	7.166
	6×6	10.26	972.6	7.115
	8×8	10.26	969.5	7.097
	10×10	10.26	968.0	7.088
	Bhaskar[54]	10.26	965.4	7.073

Table 4: Displacement and stress evaluation of three-layer composite square plates with various a/h subjected to thermal load, obtained with LW models. Assumed linear and calculated profiles are used.

$^a/_h$	Model	Assumed profiles			Calculated profiles			N_{exp}
		$^{\S}\bar{w}$	$^{\dagger}\bar{\sigma}_{xx}$	$^{\ddagger}\bar{\sigma}_{xz}$	$^{\S}\bar{w}$	$^{\dagger}\bar{\sigma}_{xx}$	$^{\ddagger}\bar{\sigma}_{xz}$	
2	SaS4	96.73	1385	64.21	48.88	456.5	30.24	10
	SaS5	96.78	1393	63.95	48.85	487.9	30.01	13
	LGD1	89.25	641.8	42.56	44.17	34.58	31.70	16
	LGD4	96.78	1393	63.95	48.85	487.9	30.01	13
	*LGD4	96.784	1389.6	63.823	48.908	488.56	30.009	13
	Bhaskar[54]	96.79	1390	63.92	–	–	–	–
10	SaS4	17.39	1029	60.66	16.40	949.4	57.18	10
	SaS5	17.39	1029	60.66	16.40	950.5	57.19	13
	LGD1	17.63	906.7	58.78	16.67	811.9	56.35	4
	LGD4	17.39	1029	60.66	16.40	950.5	57.19	13
	*LGD4	17.392	1026.3	60.540	16.395	947.96	57.070	13
	Bhaskar[54]	17.39	1026	60.54	–	–	–	–
100	SaS4	10.26	968.0	7.088	10.25	967.2	7.084	10
	SaS5	10.26	968.0	7.088	10.25	967.2	7.084	13
	LGD1	10.91	895.7	6.883	10.91	894.6	6.880	4
	LGD4	10.26	968.0	7.088	10.25	967.2	7.084	13
	*LGD4	10.260	965.37	7.0732	10.253	964.55	7.0688	13
	Bhaskar[54]	10.26	965.4	7.073	–	–	–	–

Variables are evaluated at: $^{\S}(\frac{a}{2}, \frac{b}{2}, \frac{h}{2})$; $^{\dagger}(\frac{a}{2}, \frac{b}{2}, \frac{h}{2})$; $^{\ddagger}(0, \frac{b}{2}, \frac{h}{6})$.

* Navier-type analytical solution.

Table 5: Displacement and stress evaluation of three-layer composite square plates with various a/h subjected to thermal load, obtained with ESL models ETn(Z). Calculated temperature profiles are used.

$^a/_h$	Model	$^{\S}\bar{w}$	$^{\dagger}\bar{\sigma}_{xx}$	$^{\ddagger}\bar{\sigma}_{xz}$	N_{exp}
2	FSDT$_c$	20.36	-281.6	22.10	2*
	ET4$_c$	49.30	411.4	23.97	5
	ET7$_c$	48.87	493.1	22.11	8
	ET3Z$_c$	50.09	405.1	23.43	5
	ET5Z$_c$	48.75	444.0	31.34	7
	ET7Z$_c$	48.79	489.6	31.01	9
	*LGD4$_c$	48.908	488.56	30.009	13
10	FSDT$_c$	17.26	962.7	26.41	2*
	ET3$_c$	15.95	919.4	34.62	4
	ET4$_c$	15.93	944.0	34.55	5
	ET3Z$_c$	16.41	924.8	50.44	5
	ET4Z$_c$	16.38	948.5	50.02	6
	*LGD4$_c$	16.395	947.96	57.070	13
100	FSDT$_c$	15.05	1193	3.071	2*
	ET3$_c$	10.25	966.8	4.149	4
	ET4$_c$	10.25	967.1	4.149	5
	ET2Z$_c$	10.25	966.3	6.656	4
	ET3Z$_c$	10.25	966.9	6.260	5
	ET4Z$_c$	10.25	967.2	6.260	6
	*LGD4$_c$	10.253	964.55	7.0688	13

Variables are evaluated at: $^{\S}(\frac{a}{2}, \frac{b}{2}, \frac{h}{2})$; $^{\dagger}(\frac{a}{2}, \frac{b}{2}, \frac{h}{2})$; $^{\ddagger}(0, \frac{b}{2}, \frac{h}{6})$.

* Navier-type analytical solution.

Table 6: Displacement and stress evaluation of three-layer composite square plates with various a/h subjected to thermal load, obtained with ESL models EExp$n$Z and ET1Exp$n$Z. Calculated temperature profiles are used.

$^a/_h$	Model	$^{\S}\bar{w}$	$^{\dagger}\bar{\sigma}_{xx}$	$^{\ddagger}\bar{\sigma}_{xz}$	N_{exp}
2	EExp3Z$_c$	48.66	429.7	30.22	5
	EExp5Z$_c$	48.50	459.0	22.06	7
	EExp7Z$_c$	48.77	472.6	37.32	9
	ET1Exp3Z$_c$	47.95	454.4	24.52	6
	ET1Exp5Z$_c$	48.74	521.3	31.09	8
	ET1Exp6Z$_c$	48.74	482.1	33.37	9
	*LGD4$_c$	48.908	488.56	30.009	13
10	EExp3Z$_c$	16.38	905.7	58.85	5
	EExp5Z$_c$	16.38	941.2	48.90	7
	EExp7Z$_c$	16.39	948.6	52.27	9
	ET1Exp3Z$_c$	16.38	960.8	50.21	6
	ET1Exp5Z$_c$	16.39	951.5	51.76	8
	*LGD4$_c$	16.395	947.96	57.070	13
100	EExp3Z$_c$	9.705	855.8	17.54	5
	EExp5Z$_c$	10.25	962.4	5.074	7
	EExp7Z$_c$	10.25	966.6	6.515	9
	ET1Exp3Z$_c$	10.25	970.3	6.254	6
	ET1Exp5Z$_c$	10.25	967.3	6.380	8
	*LGD4$_c$	10.253	964.55	7.0688	13

Variables are evaluated at: $^{\S}(\frac{a}{2}, \frac{b}{2}, \frac{h}{2})$; $^{\dagger}(\frac{a}{2}, \frac{b}{2}, \frac{h}{2})$; $^{\ddagger}(0, \frac{b}{2}, \frac{h}{6})$.

* Navier-type analytical solution.

Table 7: Displacement and stress evaluation of three-layer composite square plates with various a/h under thermal load, obtained with ESL models ESnCnZ and ET1SnCnZ. Calculated temperature profiles are used.

$^a/_h$	Model	$^{\S}\bar{w}$	$^{\dagger}\bar{\sigma}_{xx}$	$^{\ddagger}\bar{\sigma}_{xz}$	N_{exp}
2	ES1C1Z$_c$	44.69	-11.88	31.46	4
	ES3C3Z$_c$	48.62	445.5	40.80	8
	ES5C5Z$_c$	48.83	494.2	30.70	12
	ET1S1C1Z$_c$	48.66	375.1	24.44	5
	ET1S3C3Z$_c$	48.84	467.8	30.67	9
	ET1S4C4Z$_c$	48.83	488.6	30.90	11
	*LGD4$_c$	48.908	488.56	30.009	13
10	ES1C1Z$_c$	12.94	430.5	58.02	4
	ES3C3Z$_c$	16.36	943.0	57.05	8
	ES5C5Z$_c$	16.39	950.3	55.54	12
	ET1S1C1Z$_c$	16.57	860.5	51.26	5
	ET1S3C3Z$_c$	16.39	946.6	53.62	9
	ET1S5C5Z$_c$	16.39	950.3	55.57	13
	*LGD4$_c$	16.395	947.96	57.070	13
100	ES1C1Z$_c$	0.4448	-349.0	8.452	4
	ES3C3Z$_c$	9.241	838.0	35.87	8
	ES5C5Z$_c$	10.25	966.9	6.981	12
	ET1S1C1Z$_c$	10.34	890.0	6.354	5
	ET1S3C3Z$_c$	10.25	964.5	6.611	9
	ET1S5C5Z$_c$	10.25	967.1	6.872	13
	*LGD4$_c$	10.253	964.55	7.0688	13

Variables are evaluated at: $^{\S}(\frac{a}{2}, \frac{b}{2}, \frac{h}{2})$; $^{\dagger}(\frac{a}{2}, \frac{b}{2}, \frac{h}{2})$; $^{\ddagger}(0, \frac{b}{2}, \frac{h}{6})$.

* Navier-type analytical solution.

Table 8: Mechanical properties of T300/5208 composite lamina

E_1(GPa)	E_2, E_3(GPa)	G_{12}, G_{13}(GPa)	G_{23}(GPa)	ν_{12}, ν_{13}	ν_{23}
181	10.3	7.17	2.39	0.28	0.43

Table 9: Hygroscopic properties of T300/5208 composite lamina [13]

β_{11} (wt.%H_2O)$^{-1}$	β_{22}, β_{33} (wt.%H_2O)$^{-1}$	D_{11} (mm^2/s)	D_{22}, D_{33} (mm^2/s)
0	0.006	2.87×10^{-8}	1.63×10^{-8}

Table 10: Displacements and stresses of the composite plates with various a/h under hygroscopic load, obtained with LW models. Linear and calculated moisture concentration profiles are used.

$^a/_h$	Model	Assumed profiles			Calculated profiles			N_{exp}
		$^{\S}w$ 10^{-3}mm	$^{\dagger}\sigma_{xx}$ MPa	$^{\ddagger}\sigma_{xz}$ MPa	$^{\S}w$ 10^{-3}mm	$^{\dagger}\sigma_{xx}$ MPa	$^{\ddagger}\sigma_{xz}$ MPa	
2	SaS4	148.2	106.6	9.387	112.1	71.42	5.609	10
	SaS5	148.2	106.5	9.461	112.1	71.42	5.609	13
	SaS6	148.2	106.5	9.462	112.1	71.41	5.612	16
	LGD1	144.0	66.79	3.996	108.3	38.04	2.821	4
	LGD4	148.2	106.5	9.461	112.1	71.42	5.609	13
	*LGD4	148.68	105.56	9.4418	112.11	71.238	5.5973	13
10	SaS4	73.08	38.75	3.021	72.39	37.97	2.966	10
	SaS5	73.08	38.75	3.021	72.39	37.97	2.967	13
	LGD1	76.59	34.22	2.167	75.91	33.02	2.146	4
	LGD4	73.08	38.75	3.021	72.39	37.97	2.967	13
	*LGD4	73.078	38.636	3.0147	72.388	37.859	2.9619	13
100	SaS4	359.1	34.09	0.3208	359.1	34.08	0.3208	10
	SaS5	359.1	34.09	0.3208	359.1	34.08	0.3208	13
	LGD1	403.1	31.00	0.2370	403.1	30.99	0.2370	4
	LGD4	359.1	34.09	0.3208	359.1	34.08	0.3208	13
	*LGD4	359.12	33.983	0.32018	359.10	33.976	0.32013	13

Variables are evaluated at: $^{\S}(\frac{a}{2}, \frac{b}{2}, \frac{h}{2})$; $^{\dagger}(\frac{a}{2}, \frac{b}{2}, \frac{h}{2})$; $^{\ddagger}(0, \frac{b}{2}, \frac{h}{6})$.

* Navier-type analytical solution.

Table 11: Displacement and stress evaluation for the composite plates with various a/h subjected to hygroscopic load, obtained with ESL models ETnZ and ET1SnCnZ. Calculated linear moisture profiles are used.

$^a/_h$	Model	$^{\S}w$ 10^{-3}mm	$^{\dagger}\sigma_{xx}$ MPa	$^{\ddagger}\sigma_{xz}$ MPa	N_{exp}
2	FSDT$_c$	23.36	1.623	1.381	2*
	ET3Z$_c$	112.9	62.44	1.611	5
	ET7Z$_c$	112.4	72.04	3.135	9
	ET11Z$_c$	112.3	71.67	3.767	13
	ET13Z$_c$	112.2	71.67	3.708	15
	ET1S3C3Z$_c$	112.4	71.64	3.257	9
	ET1S5C5Z$_c$	112.2	71.61	3.737	13
	*LGD4$_c$	112.10734	71.238	5.5973	13
10	FSDT$_c$	70.44	44.93	0.7585	2*
	ET5Z$_c$	72.38	37.93	1.790	7
	ET9Z$_c$	72.39	38.01	2.198	11
	ET11Z$_c$	72.39	38.00	2.272	13
	ET1S3C3Z$_c$	72.39	37.89	2.085	9
	ET1S5C5Z$_c$	72.39	37.99	2.263	13
	*LGD4$_c$	72.388142	37.859	2.9619	13
500	FSDT$_c$	643.4	49.08	0.08121	2*
	ET5Z$_c$	359.1	34.08	0.1976	7
	ET9Z$_c$	359.1	34.08	0.2409	11
	ET11Z$_c$	359.1	34.08	0.2487	13
	ET1S3C3Z$_c$	359.1	33.96	0.2290	9
	ET1S5C5Z$_c$	359.1	34.08	0.2478	13
	*LGD4$_c$	359.099	33.976	0.32013	13

Variables are evaluated at: $^{\S}(\frac{a}{2}, \frac{b}{2}, \frac{h}{2})$; $^{\dagger}(\frac{a}{2}, \frac{b}{2}, \frac{h}{2})$; $^{\ddagger}(0, \frac{b}{2}, \frac{h}{6})$.

* Navier-type analytical solution.

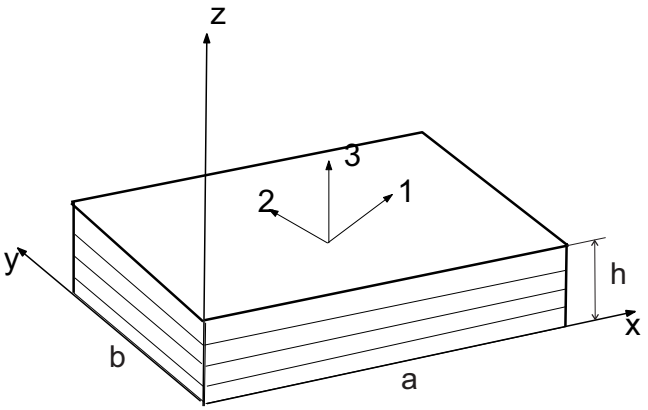

Figure 1: Multilayered plate: geometry and reference system.

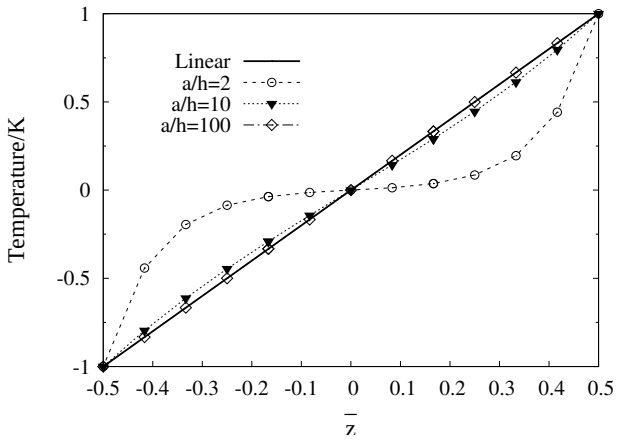

Figure 2: Temperature profiles $\bar{\theta}_A$ for composite plates of various thickness ratios (a/h), subjected to thermal load.

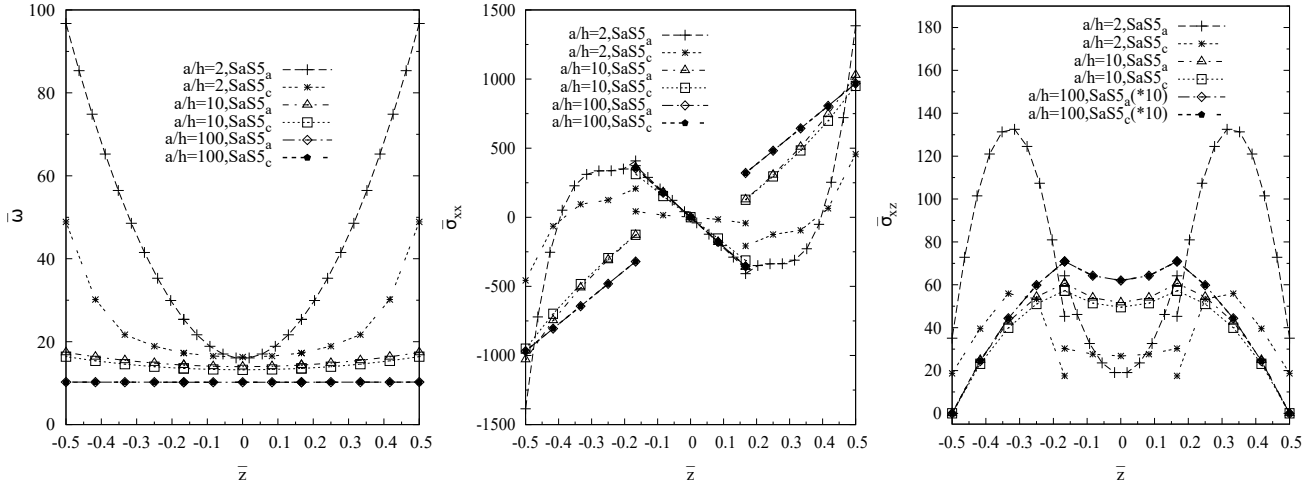

(a) $\bar{w}$ (b) $\bar{\sigma}_{xx}$ (c) $\bar{\sigma}_{xz}$

Figure 3: Transverse displacement w and stress evaluation through the thickness of the composite plates with various a/h ratios subjected to thermal load, SaS5 solutions with both linear and calculated profiles.

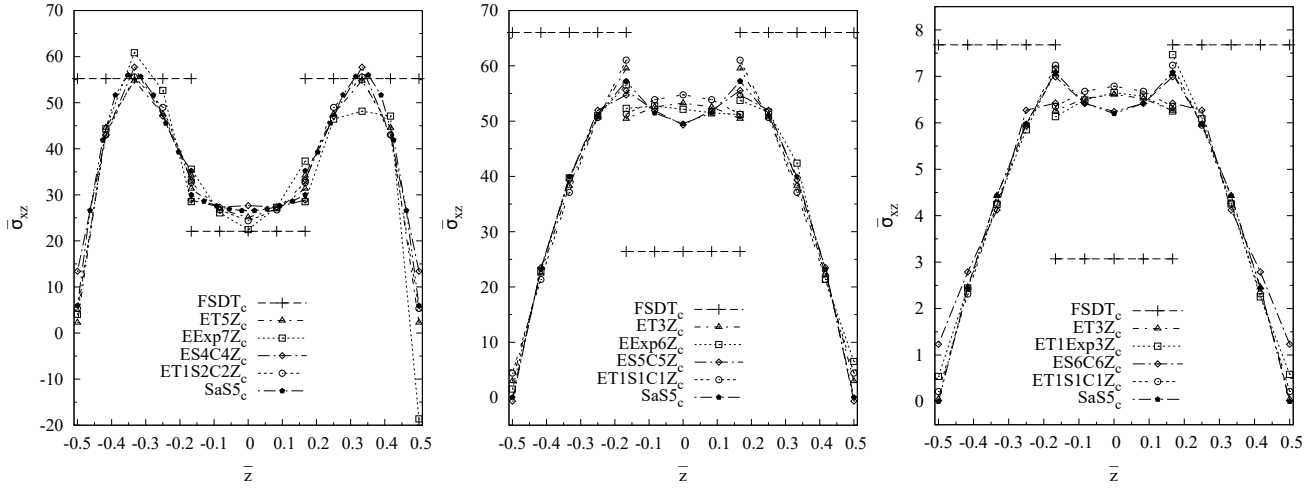

(a) $a/h = 2$ (b) $a/h = 10$ (c) $a/h = 100$

Figure 4: Transverse shear stress $\bar{\sigma}_{xz}$ through the thickness of the composite plates with various a/h ratios subjected to thermal load, obtained by ESL models adopting various thickness functions, calculated temperature profiles are used.

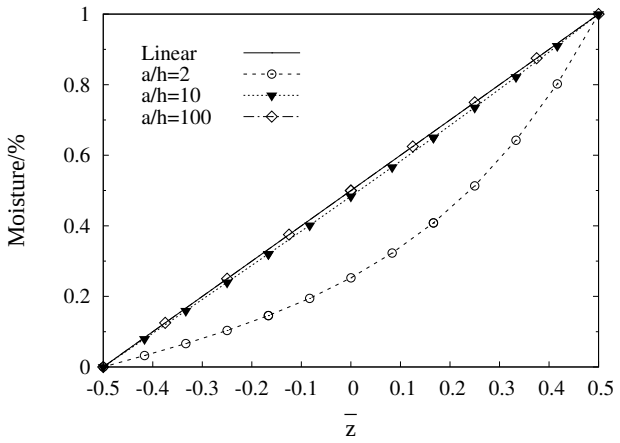

Figure 5: Moisture concentration profiles of composite plates with various (a/h) ratios.

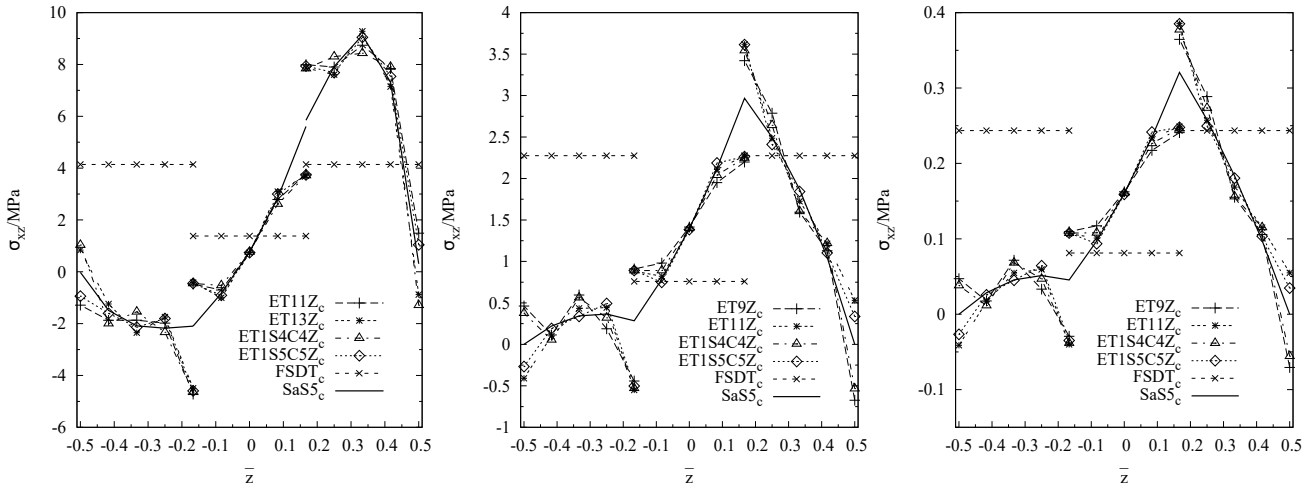

(a) $a/h = 2$ (b) $a/h = 10$ (c) $a/h = 500$

Figure 7: Transverse shear stress σ_{xz} through the thickness of the composite plates with various a/h under hygroscopic load, obtained by adopting various thickness functions, both linear and calculated temperature profiles are used.

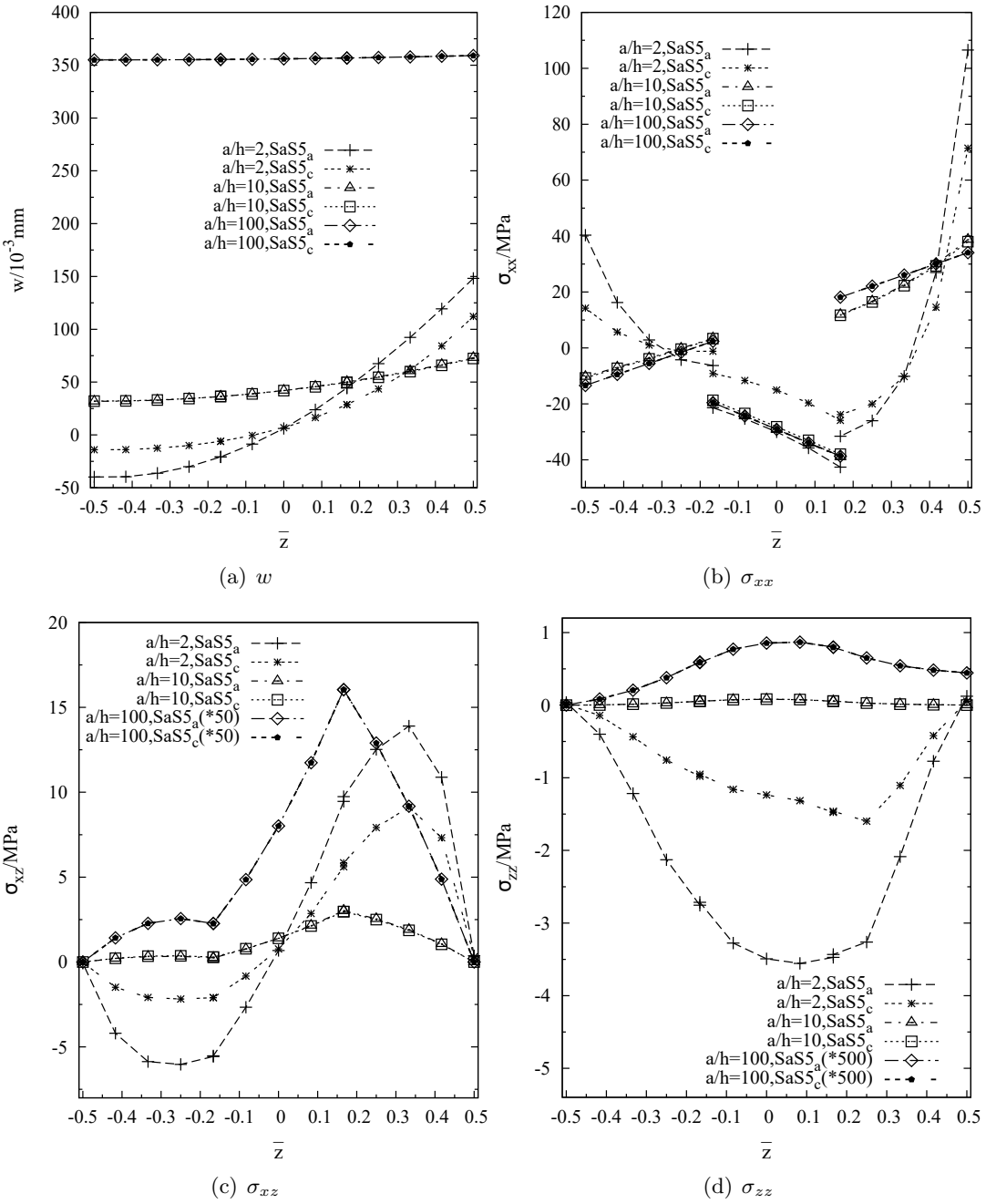

(a) w (b) σ_{xx}

(c) σ_{xz} (d) σ_{zz}

Figure 6: Transverse displacement w and stresses through the thickness of the composite plates with various a/h ratios under hygroscopic load, SaS5 solutions with both linear and calculated profiles.